Temperature profile of GaInAs/AlInAs/InP quantum cascade-laser facets measured by microprobe photoluminescence

Vincenzo Spagnolo, Mariano Troccoli, and Gaetano Scamarcio[a)]
INFM, Dipartimento Interateneo di Fisica, Università e Politecnico di Bari, via Amendola 173, 70126 Bari, Italy

Claire Gmachl, Federico Capasso, Alessandro Tredicucci, A. Michael Sergent, Albert L. Hutchinson, Deborah L. Sivco, and Alfred Y. Cho
Bell Laboratories, Lucent Technologies, 600 Mountain Avenue, Murray Hill, New Jersey 07974

(Received 18 September 2000; accepted for publication 5 February 2001)

The local temperature of quantum-cascade lasers operating in continuous wave mode is reported. This information is extracted from the thermal shift of the band-to-band photoluminescence peaks in the AlInAs and InP cladding layers of quantum-cascade laser facets using a high-resolution microprobe setup. Interpolation by means of a two-dimensional heat diffusion model allows to obtain the temperature profile and the thermal conductivity in the waveguide core. Comparison between substrate and epilayer-side mounted lasers shows the superior thermal dissipation capability of the latter, and explains their better performance with respect to threshold current and maximum operating temperature.
[DOI: 10.1063/1.1359146]

Quantum cascade (QC) lasers are unipolar semiconductor devices based on transitions between conduction subbands[1] or minibands[2] of multiple quantum well structures. Since their invention, the continuous optimization of the active region and waveguide design has led to great improvements in terms of available wavelengths (3–19 μm), peak and average optical power, threshold currents, single mode operation, and maximum operating temperature.[3–7] At present, lasing up to 425 K in pulsed mode,[6] and 175 K in continuous wave (cw) has been reported.[7] This performance makes QC lasers an almost ideal compact source of midinfrared radiation for gas sensing applications.[8] However, it would be highly desirable to raise the cw operating temperature above $\sim$250 K, in a range accessible to thermoelectric coolers. For further improvements one has to contend the large dissipated electrical power, typically 10–50 kW/cm^2, and the low thermal conductivity of QC laser materials. The latter is mainly due to the large number of interfaces (300–1200) and the high thermal resistance of GaInAs or AlInAs materials.

In this letter we present the experimental determination of local heating of QC lasers during cw operation. We used a microprobe photoluminescence technique[9] to compare epilayer and substrate-side mounted devices with identical laser structure, in the heat sink temperature range $T_H = 100-190\,$K. In conventional diode lasers the facet temperature can be significantly higher than that in the device core because of nonradiative surface electron-hole recombination processes.[10,11] The absence of this effect in unipolar devices such as QC lasers allows us to use the facet temperature as a close estimate of the internal one. Our results show the superior thermal dissipation capability of epilayer-side mounted devices, which explain their better laser performance.[7]

For the present study we chose the GaInAs/AlInAs laser structure of Ref. 5 (wafer D2405) which shows the best thermal performance in cw operation to date.[7] The waveguide core consists of an $\sim$0.53 μm thick stack of twelve active regions with interleaved injector regions sandwiched between two 0.5 μm thick $Ga_{0.47}In_{0.53}As$ layers. The top cladding layer is formed by an inner 2.5 μm thick $Al_{0.48}In_{0.52}As$ layer doped to $n = 1-2\times10^{17}\,cm^{-3}$ and an outer 0.5 μm thick $Ga_{0.47}In_{0.53}As$ layer heavily doped to $n = 5\times10^{18}\,cm^{-3}$ for plasmon-enhanced confinement. The InP substrate, doped to $n = 2\times10^{17}\,cm^{-3}$, acts as a lower waveguide cladding layer. The three-coupled wells active region was designed for emission at 8 μm wavelength. The devices were processed into 2.5 mm long, 11 μm wide, deep-etched ridge waveguides and then mounted either substrate or epilayer-side onto copper holders using In solder as schematically shown in Figs. 1(a) and 1(b). To avoid facets overheating and the formation of ''hot spots,'' the solder bonding was extended to the very end of the laser ridge using the procedure described in Ref. 7. The devices were then mounted into a helium flow microcryostat and kept at a controlled heat sink temperature, measured with a calibrated Si diode mounted on the copper cold finger close to the laser.

The photoluminescence (PL) signal was obtained by focusing the 476.2 nm line of a Kr^+ laser onto the QC laser front facet to a spot of $\sim$1 μm diameter with an 80$\times$ microscope objective. The sample position relative to the Kr^+ laser spot was varied with a piezoelectric x-y stage and controlled with 0.1 μm precision. Laser induced heating of the samples was avoided keeping the incident power density $<10^4$ W/cm^2. The PL signal was dispersed using a 0.64 m monochromator and detected with a Si charge coupled device detector (CCD) cooled to 140 K, with a long-wavelength cutoff of $\sim$1 μm.

At each point, the temperature of the laser facet is determined by comparing the shift of the PL peak to a calibration curve measured for each layer with no current through the

[a)]Author to whom correspondence should be addressed; electronic mail: scamarcio@fisica.uniba.it

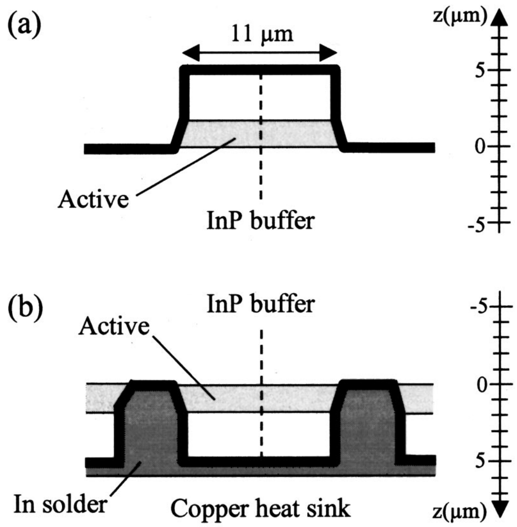

FIG. 1. Schematics of QC laser facets for epilayer-side (a) and substrate-side (b) mounted devices. The dashed lines indicate the locations investigated by microprobe photoluminescence. The lightly shaded regions indicate the waveguide core. The dark shaded region shows the indium solder. The origin of the z axis corresponds to the interface between the waveguide core and the InP substrate. Positive values indicate the direction towards the AlInAs cladding layers.

device. Figures 2(a) and 2(b) compare the typical photoluminescence spectra of the AlInAs top cladding layer and the InP substrate obtained with device-off or device-on. The PL peak energy E_p was accurately determined by fitting a second-order polynomial to the PL spectrum in a 20 meV range around E_p. The calibration curves of Figs. 2(c) and 2(d) are obtained for AlInAs and InP layers by probing the device at zero current while varying the heat sink temperature. The continuous lines are best fitting curves obtained with the empirical relation $E_p(T)=E_p(0)-\alpha T^2/(\beta+T)$, similar to that usually giving excellent reproduction of the band-gap temperature dependence. The rather strong temperature dependence of AlInAs and InP band gaps ($dE_g/dT\sim 0.25$ meV/K) at temperatures above 70 K allows

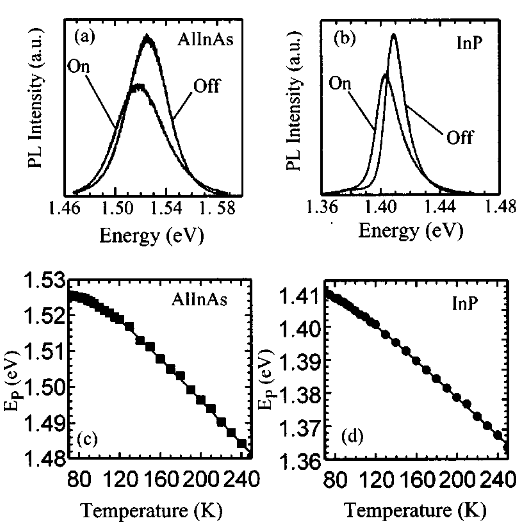

FIG. 2. Characteristic photoluminescence spectra measured at $T_H=80$ K with a microprobe setup from a QC laser facet with the device ''on'' (cw injected current $I=0.9$ A) and ''off'' ($I=0$). (a) AlInAs upper cladding layer; (b) InP lower cladding. Temperature dependence of the AlInAs (c) and InP (d) photoluminescence peak position.

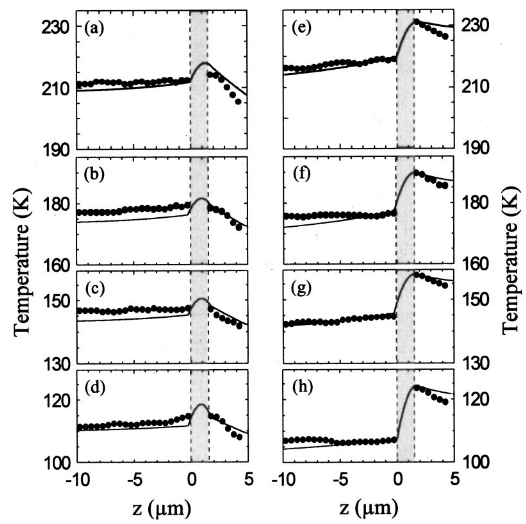

FIG. 3. (a)–(h) experimental (●) and calculated (solid lines) temperature profiles of epilayer-(a)–(d) and substrate-side (e)–(h) mounted QC lasers driven by a cw electrical power of 3.2 W. The heat sink temperatures are $T_H=190$ K (a), (e), $T_H=160$ K (b), (f), $T_H=130$ K (c), (g), and $T_H=100$ K (d), (h).

a temperature resolution <0.3 K. Note that this is much better than achievable with microprobe Raman technique (± 10 K) using the ratio between anti-Stokes and Stokes intensity bands.[12] Unfortunately, the PL emission at ~ 1.5 μm from GaInAs layers or at ~ 1.4 μm from GaInAs/AlInAs heterostructures in the waveguide core cannot be detected because of the long-wavelength cutoff of our apparatus.

The local temperatures measured at different positions along the facet center axis for an epilayer and a substrate-side mounted device are shown in Figs. 3(a)–3(d) and Figs. 3(e)–3(h), respectively. The heat sink temperature is varied in the range $T_H=100-190$ K, while a constant cw electrical power $P=3.2$ W is dissipated in the device. The measured temperatures are always higher (by 7–21 K) than T_H because of the finite thermal resistance of the device. The main distinction between the two lasers is the temperature difference across the waveguide core $\Delta T_w=T(z=1.5\,\mu\mathrm{m})-T(z=0)$, which can be related to the thermal resistance along the z axis. In the range $T_H=100-190$ K, we found $\Delta T_w=10-16.5$ K in the substrate-side mounted device [Figs. 3(e)–3(h)] and $\Delta T_w\sim 0$ in the epilayer-side mounted one [Figs. 3(a)–3(d)]. This means that in the epilayer-side mounted device, the thermal resistances in the two directions $z<0$ and $z>1.5$ μm [see Fig. 1(b)] are comparable. On the other hand, the thermal resistance in the direction $z>1.5$ μm is much larger in the substrate-side mounted laser, due to the absence of an effective thermal contact between the top of the ridge and the heat sink.

Knowledge of the heat conductivity of the active region, k_w, and of its dependence on temperature and doping level would allow to calculate the heat fluxes and the local temperatures inside the active region. The latter piece of information is very difficult to obtain by independent means in a complex multilayered structure like ours. To our knowledge, no investigation of the GaInAs/AlInAs or similar ternary–ternary heterostructures has been reported so far, and the use of bulk values is a too rough approximation. In fact, due to the presence of interfaces and inherent phonon interference

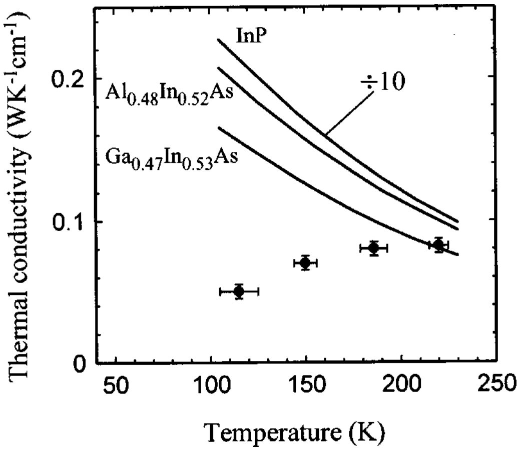

FIG. 4. Thermal conductivity of the active region of QC lasers (dots) extracted by fitting a two-dimensional model of heat diffusion to the experimental data of Figs. 3(e)–3(h). The continuous lines are calculated using $(4.06-0.020\times T+2.88\times 10^{-5}\times T^2)$ W/(K cm) for the heat conductivity of InP and $(0.29-0.00139\times T+1.98\times 10^{-6}\times T^2)$ W/(K cm) for the heat conductivity of $Ga_{0.47}In_{0.53}As$ (Refs. 7 and 16). The relation for GaInAs is extracted from known values at selected temperatures. The heat conductivity of $Al_{0.48}In_{0.52}As$ is scaled by a factor 1.25 with respect to that of GaInAs, based on the known heat conductivity values of GaAs, AlAs, and InAs.

effects, the heat conductivity of semiconductor superlattices may be considerably smaller than that of constituent materials and has been found to be either an increasing function, as in Si/Ge,[13] or a decreasing function of the temperature, as in GaAs/AlAs superlattices.[14] Existing theories do not fully explain the observed temperature dependence even in the prototype GaAs/AlAs system.[15] Therefore, in order to estimate k_w, we fitted a two-dimensional model of heat diffusion to the experimental results of Figs. 3(e)–3(h), employing a commercial software package. We used the values plotted in Fig. 4 for the heat conductivity of InP, GaInAs, and AlInAs. For the insulating layer, contact layer, and solder we used 0.1, 0.87, and 3.2 W/(K cm), respectively. As boundary conditions we used the heat sink temperature. For the substrate-side mounted device, we found best agreement with the k_w values of Fig. 4. These results show that the thermal conductivity of the active region is significantly lower than that of bulk GaInAs and AlInAs, and that it is an increasing function of T in the temperature range 110–210 K. The heat flux towards the InP substrate turns out to be 85%–95% of the total power. The residual power flows out of the active region into the AlInAs cladding or laterally into the gold layer and eventually flows back into the InP substrate.

The curves in Figs. 3(a)–3(d), calculated for the epilayer-side mounted devices using k_w values interpolated from those of Fig. 4, are in good agreement with the experimental temperatures in the cladding layers. Our 2D calculations show that the heat extraction through the AlInAs cladding is greatly enhanced in the epilayer-side mounted device. Still, ~60% of the heat flows toward the InP substrate before reaching the heat sink through lateral channels, due to the high thermal conductivity of InP. The calculated average temperature in the active region of the epilayer-side mounted laser is always lower than that of the substrate-side mounted one, and this temperature difference increases with T_H. These results explain the superior device performances of epilayer-side mounted QC lasers, in terms of maximum operating temperature and threshold current density.[7]

In conclusion, we have shown that thermal modeling of GaInAs/AlInAs/InP QC lasers, based on the measurement of facet temperature profile and 2D heat diffusion calculations, allows to determine the active region thermal conductivity and gives a reliable description of the device thermal characteristics. This approach will allow to design QC laser structures with improved heat dissipation capability. Better results, considering structures including InP top cladding layers[7] or buried waveguides, are expected.

This work was partly supported by INFM Project PRA-SUPERLAS and MURST-CIPE cl. 26-P5WP2. The work performed at Bell Laboratories was partially supported by DARPA/U.S. Army Research Office under Grant Nos. DAA-G-55-98-C-0050 and DAAD19-00-C-0096.

[1] J. Faist, F. Capasso, D. L. Sivco, C. Sirtori, A. L. Hutchinson, and A. Y. Cho, Science **264**, 553 (1994).
[2] G. Scamarcio, F. Capasso, C. Sirtori, J. Faist, D. L. Sivco, A. L. Hutchinson, and A. Y. Cho, Science **276**, 773 (1997).
[3] F. Capasso, A. Tredicucci, C. Gmachl, D. L. Sivco, A. L. Hutchinson, A. Y. Cho, and G. Scamarcio, IEEE J. Sel. Top. Quantum Electron. **5**, 792 (1999).
[4] A. Tredicucci, F. Capasso, C. Gmachl, D. L. Sivco, A. L. Hutchinson, and A. Y. Cho, IEEE Photonics Technol. Lett. **12**, 260 (2000).
[5] C. Gmachl, F. Capasso, A. Tredicucci, D. L. Sivco, R. Köhler, A. L. Hutchinson, and A. Y. Cho, IEEE J. Sel. Top. Quantum Electron. **5**, 808 (1999).
[6] C. Gmachl, A. Tredicucci, F. Capasso, A. L. Hutchinson, D. L. Sivco, A. M. Sergent, T. Mentzel, and A. Y. Cho, Electron. Lett. **23**, 723 (2000).
[7] C. Gmachl, A. M. Sergent, A. Tredicucci, F. Capasso, A. L. Hutchinson, D. L. Sivco, J. N. Baillargeon, S. N. G. Chu, and A. Y. Cho, IEEE Photonics Technol. Lett. **11**, 1369 (1999).
[8] C. Gmachl, F. Capasso, R. Köhler, A. Tredicucci, A. L. Hutchinson, D. L. Sivco, J. N. Baillargeon, and A. Y. Cho, IEEE Circuits Devices **16**, 10 (2000).
[9] D. C. Hall, L. Goldberg, and D. Mehuys, Appl. Phys. Lett. **61**, 384 (1992).
[10] R. Schatz and C. G. Bethea, J. Appl. Phys. **76**, 2509 (1994).
[11] R. Puchert, A. Bärwolff, U. Menzel, A. Lau, M. Voss, and T. Elsaesser, J. Appl. Phys. **80**, 5559 (1996).
[12] W. C. Tang, H. J. Rosen, P. Vettiger, and D. J. Webb, Appl. Phys. Lett. **58**, 557 (1991).
[13] S. M. Lee, D. G. Cahill, and R. Venkatasubramanian, Appl. Phys. Lett. **70**, 2957 (1997).
[14] W. S. Capinski, H. G. Maris, T. Ruf, M. Cardona, K. Ploog, and D. S. Katzer, Phys. Rev. B **59**, 8105 (1999).
[15] G. Chen, Phys. Rev. B **57**, 14958 (1998).
[16] *Landolt-Börnstein Tables*, edited by O. Madelung, M. Schultz, and H. Weiss (Springer, Berlin, 1982), Group III, Vol. 17a.